ELSEVIER

Ultramicroscopy 74 (1998) 7–26

ultramicroscopy

An optical potential approach to incoherent multiple thermal diffuse scattering in quantitative HRTEM

Z.L. Wang*

School of Materials Science and Engineering, Georgia Institute of Technology, Atlanta, GA 30332-0245, USA

Received 26 September 1997; received in revised form 17 February 1998

Abstract

The theory for the absorption potential (or optical potential) in electron scattering was first proposed by Yoshioka in 1957 based on an approximation that the Green's function is replaced by its form in free-space. This approximation has dramatically simplified the calculation, but the function of the optical potential has been partially lost. In this paper, a rigorous theoretical proof is given based on the quantum inelastic excitation theory to show that the inclusion of the optical potential in the dynamic calculation automatically recovers the contributions made by the high-order diffuse scattering although the calculation is done using the equation derived for single diffuse scattering. This conclusion generalizes the existing first-order diffuse scattering theories to cases in which the incoherent multiple diffuse scattering are important. It is suggested that multiple thermal diffuse scattering (or phonon excitations) is likely to be the dominant source for affecting image contrast in quantitative electron microscopy because of the channeling effect and the localized scattering nature of phonon excitation. Surprisingly, phonon scattering is anticipated to contribute fine atomic-scale contrast in the image, which is believed to be more pronounced than the "white noise" effect of conventional understanding. The optical potential is no longer a simple potential function, rather it is a non-local function strongly dependent on the dynamic diffraction in the crystal because of the involvement of Green's function. These characteristics can be properly taken into the computation using a proposed Bloch wave–multislice approach, in which the non-local effect is resolved in the Bloch wave matrix diagonalization and the dynamical effect is taken care of using Green's function calculated by the multislice theory under the small angle (or high-energy) scattering approximation. In the ground-state approximation, by which we mean that the crystal is in its ground state before each and every inelastic excitation, an introduction of the mixed dynamic form factor and the density matrix automatically produces the incoherence between different order and different phonon excitation processes, resolving a big problem encountered by many other theories. In the conventional dynamical calculation for elastic wave, the inclusion of the Debye–Waller factor and the optical potential accounts only for the effects of the phonon excitation on the elastic wave rather than the contribution made by the diffusely scattered electrons to the image/diffraction pattern. © 1998 Elsevier Science B.V. All rights reserved.

PACS: 61.16.B; 25.30.D; 72.10

Keywords: Optical potential; Thermal diffuse scattering; Density matrix; High resolution transmission electron microscopy; Multislice theory; Bloch wave theory

*E-mail: zhong.wang@mse.gatech.edu.

0304-3991/98/$19.00 © 1998 Elsevier Science B.V. All rights reserved.
PII: S0304-3991(98)00020-5

1. Introduction

The "absorption" potential, or the so called optical potential, is an important factor in quantitative dynamical calculations for electron diffraction and imaging [1,2]. Optical potential was introduced in electron diffraction over four decades ago [3–5], and it can account for the effect of inelastic scattering, such as plasmon excitation, atomic inner-shell excitation and phonon (or thermal diffuse) scattering, on the elastically scattered wave [6–9]. This potential is usually approximated as an imaginary function and it is responsible for the reduction of the Bragg scattered intensity. In recent years the commercialization of electron energy-filter in transmission electron microscopy (TEM) has greatly affected quantitative electron microscopy, using which electrons with energy-loss larger than a few eV can be removed from the image or diffraction pattern except the phonon scattered electrons. It is therefore inevitable to involve phonon scattered electrons in data analysis, but the multiple phonon excitation theory in electron diffraction is not yet well established.

Thermal diffuse scattering (TDS) not only reduces the Bragg scattered intensity, which is equivalent to introducing a Debye–Waller factor and an optical potential in the calculation, but it also gives a well defined "background" pattern in the diffraction plane. If one is interested only in the Bragg reflected intensity, an introduction of both Debye–Waller factor and the optical potential is essential to fit the data. If one is also interested in the distribution of phonon scattered electrons in reciprocal space, a rigorous theoretical calculation must be performed. Most of the theories currently available can only, however, take into account the first-order diffuse scattering, while the high-order diffuse scattering are dropped [2]. This problem may become severe in quantitative fitting of high-resolution TEM images because TDS is believed to be responsible for the disagreement between the calculated images and the observed images [10].

Dynamic calculation of multiple TDS with consideration of incoherence is a rather difficult problem. Calculations using the "frozen" lattice model has been frequently performed in the multislice theory following two different approaches. One approach assumes that the entire crystal in one vibration configuration is a frozen lattice and the diffuse scattering generated in the entire volume is coherent, but the final intensity is an incoherent sum over the intensities contributed by different lattice configurations [11,12]. The other approach assumes that the diffuse scattering generated within one thin crystal slice is coherent, but incoherence is preserved for the scattering generated from different slices [13,14]. The former has properly considered the multiple diffuse scattering effect but partially ignored the incoherence between the different orders of diffuse scattering. The latter treats the incoherence properly but the higher order diffuse scattering is neglected. Recent studies have shown that the introduction of the mixed dynamic form factor $S(\boldsymbol{Q}, \boldsymbol{Q}')$ can properly account for the incoherence between different orders of TDS [15].

In this paper, we try to answer three questions: (1) what is the nature of the optical potential? (2) What can it be used for? and (3) how can it be precisely calculated? These questions seem easy at the first sight, but in fact they have profound truth beyond conventional understanding because the approximation made for deriving the potential has never been re-examined. Using the formal inelastic excitation theory of Yoshioka [3], a rigorous proof is given to show that the high-order diffuse scattering can be recovered in the calculation using the first-order diffuse scattering equation, provided the correct optical potential is included in the calculation of the elastic wave. It is shown that the incoherence between different orders of diffuse scattering is automatically included with the use of the mixed dynamic form factor. The precise form of the optical potential is given and its calculation is proposed based on a Bloch wave – multislice approach.

2. The "absorption" potential introduced by Yoshioka

The absorption potential in electron diffraction was formally introduced by Yoshioka in consideration of the effects of an inelastic scattering on an elastically scattered wave. Phonon excitation is an inelastic

scattering process that is most adequately described using the Yoshioka's approach [3], in which the quantum nature of phonons and the incoherence effects are adequately treated. In this theory the eigenstate of the incident electron-crystal system is expressed as a product of the eigenstate of the crystal with that of the incident electron,

$$\Phi_s(\boldsymbol{r}, \boldsymbol{R}) = \sum_{n=0}^{\infty} a_n(\boldsymbol{R})\Psi_n(\boldsymbol{r}), \tag{1}$$

where a_n is the nth eigenstate of the crystal of energy ε_n; Ψ_0 is the elastic scattered wave of energy E, and Ψ_n is the inelastically scattered wave of energy $E_n = E - \varepsilon_n$ after exciting the nth crystal state; $\boldsymbol{R}$ represents the coordinates of crystal electrons $(\boldsymbol{r}_1, \ldots, \boldsymbol{r}_M)$. The fundamental equations which govern the generation, scattering and transition between/among the elastic wave and the inelastic waves are:

$$\left[\left(-\frac{\hbar^2}{2m_0}\nabla^2 + H_{00} - E\right)\right]\Psi_0 = -\sum_{m=1} H_{0m}\Psi_m, \tag{2a}$$

$$\left[\left(-\frac{\hbar^2}{2_{m0}}\nabla^2 + H_{nn} - E_n\right)\right]\Psi_n = -\sum_{m\neq n} H_{nm}\Psi_m, \tag{2b}$$

where the transition matrix from state a_m to a_n is

$$H_{nm} = \int a_n^* H a_m \, \mathrm{d}\boldsymbol{R} = \langle a_n|H|a_m\rangle, \tag{2c}$$

and H is the interaction Hamiltonian between the incident electron with the electrons and nuclei in the crystal.

Phonon excitation is a quantum transition process, in which both the creation and annihilation of phonons are possible. The excitation process can be adequately described using the transition matrix, similar to the other inelastic electron transitions. Phonon excitation has the following characteristics. First, the phonon energy is in the order of 0.1 eV or less, very much smaller than the incident energy of the electron (typically of 100 keV), thus, the electron energy can be considered to be unperturbed by the energy transfer in phonon excitation, which means $E_n \approx E$, but this energy loss has destroyed the coherence of the electron. Hence, *the incoherence among all the crystal states* (*e.g.*, *different phonon states*) *must be preserved*. Secondly, a phonon is characterized by a group of quantities of $(\boldsymbol{q}, \omega_j, \boldsymbol{e})$, where $\boldsymbol{q}$ is the phonon wave vector, ω_j the phonon frequency belonging to the jth branch and $\boldsymbol{e}$ the polarization vector, which means that an excited state a_n is also characterized by $(\boldsymbol{q}, \omega_j, \boldsymbol{e})$. Finally, the interaction Hamiltonian of the electron with the crystal is determined by the instantaneous crystal potential V:

$$V(\boldsymbol{r}) = \sum_i V_i(\boldsymbol{r} - \boldsymbol{r}_i - \boldsymbol{u}_i), \tag{3}$$

where $\boldsymbol{r}_i$ is the equilibrium position of the ith atom and $\boldsymbol{u}_i$ is its displacement. The diagonal matrix element H_{nn} is

$$H_{nn} \approx H_{00} = -e\langle n_s(\boldsymbol{q}, \omega_j)|V(\boldsymbol{r})|n_s(\boldsymbol{q}, \omega_j)\rangle, \tag{4a}$$

where and $|n_s(\boldsymbol{q}, \omega_j)\rangle$ characterizes the phonon state of the crystal with n_s standing for the number of phonons in the state. Using electron scattering factor, one has

$$\begin{aligned} H_{00} &= -e\langle n_s(\boldsymbol{q}, \omega_j)|\sum_i V_i(\boldsymbol{r} - \boldsymbol{r}_i - \boldsymbol{u}_i)|n_s(\boldsymbol{q}, \omega_j)\rangle \\ &= -e\sum_i \int \mathrm{d}\tau f_i^e(\tau)\exp[2\pi\mathrm{i}\boldsymbol{\tau}\cdot(\boldsymbol{r} - \boldsymbol{r}_i)]\langle n_s(\boldsymbol{q}, \omega_j)|\exp(-2\pi\mathrm{i}\boldsymbol{\tau}\cdot\boldsymbol{u}_i)|n_s(\boldsymbol{q}, \omega_j)\rangle \\ &= -e\sum_i \int \mathrm{d}\tau f_i^e(\tau)\exp[2\pi\mathrm{i}\boldsymbol{\tau}\cdot(\boldsymbol{r} - \boldsymbol{r}_i)]\exp[-W_i(\tau)] = -eV_0, \end{aligned} \tag{4b}$$

where the Debye–Waller factor is $W_i = 2\pi^2\langle n_s|(\boldsymbol{\tau}\cdot\boldsymbol{u}_i)^2|n_s\rangle$. Therefore, H_{00} is the "time" averaged crystal potential (V_0) as characterized by the Debye–Waller factor. This means that *the Debye–Waller factor must be introduced in any calculation regardless of whether the inelastically scattered electrons are included or not*. The Yoshioka's equations are a more generalized approach, which can include, in principle, several different types of inelastic excitation events, such as plasmon excitation, atomic inner-shell excitation and phonon excitation. Although a general solution can be found in the multislice approach [16], but its calculation becomes too large to be carried out. If all of the inelastic excitations with energy-loss larger than a few eV are removed from the image/diffraction pattern by an energy filter, we need to focus only on phonon excitation.

To properly consider the incoherence between different phonon excitation processes, we only consider a multiple phonon excitation process as illustrated in Fig. 1. This diagram is given based on the so-called "*ground state*" *approximation* [15]. In one-particle multiple scattering theory, each time the electron inelastically interacts with the crystal atoms the collision is assumed to take place in such a way as if the crystal is in its ground state, and the effect of previous collisions on the crystal is negligible. This condition is satisfied if $\tau_0 v > \Lambda$, where τ_0 is the lifetime of the crystal excitation state and Λ is the electron mean-free-path length. For a 100 keV electron and the phonon life time $\tau_0 \approx 10^{-13}$s, $\tau_0 v = 15$ μm, and for phonon scattering Λ is 50–300 nm depending on elements. The condition of $\tau_0 v > \Lambda$ is absolutely satisfied. Therefore, *there is no phonon decay during the interaction of the electron with the crystal, and the crystal can be assumed in its ground state before any quantum excitation.*

The ground-state approximation simply means that we can ignore the transition among different excited states except the ground state. Eq. (4b) is approximated as

$$\left[\left(-\frac{\hbar^2}{2m_0}\nabla^2 - eV_0 - E\right)\right]\Psi_n \approx -H_{n0}\Psi_0. \tag{5a}$$

This is actually the first-order diffuse scattering equation. *We first make this approximation, then we will prove that the inclusion of an optical potential in* Eqs. (2a)–(2e) *can recover all of the high order scattering terms dropped here*. This is the core of this paper. Eq. (5a) can be converted into an integral equation

$$\Psi_n(\boldsymbol{r}) = -\int \mathrm{d}\boldsymbol{r}_1\, G(\boldsymbol{r},\boldsymbol{r}_1)H_{n0}(\boldsymbol{r}_1)\Psi_0(\boldsymbol{r}_1), \quad \text{for } n>0 \tag{5b}$$

where G is Green's function satisfying

$$\left(-\frac{\hbar^2}{2m_0}\nabla^2 - eV_0 - E\right)G(\boldsymbol{r},\boldsymbol{r}_1) = \delta(\boldsymbol{r}-\boldsymbol{r}_1). \tag{5c}$$

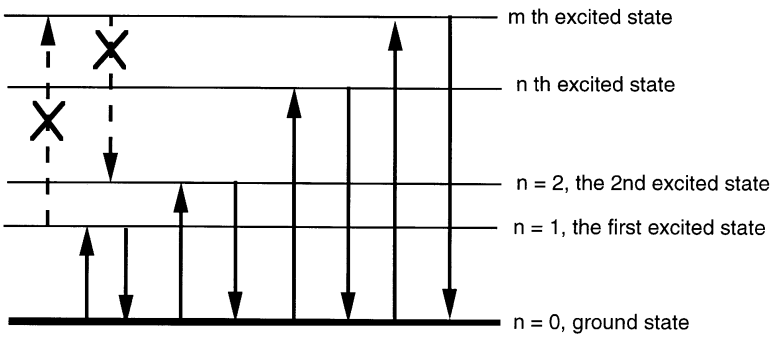

Fig. 1. A schematic model showing quantum transition in crystal state under the ground-state approximation.

Substituting Eq. (5b) into Eq. (4a), yields

$$\left[\left(-\frac{\hbar^2}{2m_0}\nabla^2 - eV_0 - E\right)\right]\Psi_0(\boldsymbol{r}) = \int \mathrm{d}\boldsymbol{r}_1\, G(\boldsymbol{r}, \boldsymbol{r}_1)\left[\sum_{m=1} H_{0m}(\boldsymbol{r})H_{m0}(\boldsymbol{r}_1)\right]\Psi_0(\boldsymbol{r}_1), \tag{6}$$

where the term on the right-hand side is equivalent to a non-local "potential" V' defined by

$$[eV'\Psi_0] = \int \mathrm{d}_1\, G(\boldsymbol{r}, \boldsymbol{r}_1)\left[\sum_{m=1} H_{0m}(\boldsymbol{r})H_{m0}(\boldsymbol{r}_1)\right]\Psi_0(\boldsymbol{r}_1). \tag{7a}$$

The optical potential given by Eq. (7a) has two important characteristics. One the V' function is a non-local function, depending on the "history" of inelastic excitation events. The other is the enrollment of dynamical diffraction in V', so it is not, in general, simply a potential function.

To make V' a potential function independent of dynamic diffraction, Yoshioka [3] made an approximation of replacing Green's function by its form in free space, thus

$$[eV'\Psi_0] \approx \frac{2m_0}{\hbar^2}\int \mathrm{d}\boldsymbol{r}_1 \frac{\exp(2\pi K_0|\boldsymbol{r} - \boldsymbol{r}_1|)}{4\pi|\boldsymbol{r} - \boldsymbol{r}_1|}\left[\sum_{m=1} H_{0m}(\boldsymbol{r})H_{m0}(\boldsymbol{r}_1)\right]\Psi_0(\boldsymbol{r}_1). \tag{7b}$$

This approximation was given in his paper but it has been forgotten in the literature, and it has been believed that Eq. (7b) is the "true" absorptive potential. The key of this approximation is that the dynamic diffraction effect is dropped in the calculation. On the other hand, the Yoshioka's approximation is very reasonable if one is interested only in the elastically scattered electrons because once the electron is diffusely scattered out of the Bragg peaks, it is considered to be "absorbed" and there is no need to consider its subsequent diffraction behavior. The dynamic diffraction after the inelastic scattering can only change the angular distribution of the electrons, but has no effect on the total inelastic scattering probability. It is sure that this approximation makes the numerical calculation much easier, but the question is what has been dropped by this approximation and what can the dropped effect be used for? This question will be answered in Section 4.

3. How important is the multiple TDS and how does it affect the image contrast?

Before proposing our formal multiple-elastic and multiple-inelastic scattering theory, one question we must answer is how important is the higher-order diffuse scattering in electron diffraction and imaging of thin specimens? Fig. 2 shows the calculated instantaneous potential V, thermal equilibrium potential V_0, and the difference $\Delta V = V - V_0$ for a silicon atom. If the instantaneous position of the atom is its equilibrium lattice site, ΔV is a symmetric, sharp function. If the atom is displaced to an instantaneous position located at 0.068 Å on the right-hand side from the equilibrium site, ΔV is no longer symmetric (Fig. 2b). It is striking to note that the magnitude of ΔV is comparable to that of V_0 and this is true for each atom present in the specimen.

To simply demonstrate the importance of thermal diffuse scattering in HRTEM, the weak phase object approximation is adopted although it is believed to be an unrealistic approximation but it is still the best model for illustrating the physics involved in the image formation. The electron wave after exiting the crystal surface can be represented by

$$\Phi(\boldsymbol{b}) \approx 1 + \mathrm{i}\sigma V_{\mathrm{p}}(\boldsymbol{b}) = 1 + \mathrm{i}\sigma V_{\mathrm{p0}}(\boldsymbol{b}) + \mathrm{i}\sigma\Delta V_{\mathrm{p}}(\boldsymbol{b}, t), \tag{7c}$$

where $\sigma = \pi/\lambda U_0$, $\boldsymbol{b} = (x, y)$, λ the electron wave length, U_0 the electron acceleration voltage, V_{p0} is the static crystal projected potential, and ΔV_{p} is the distorted potential introduced by atom vibration. In the "frozen" lattice model (this model is used only here for simplifying the discussion), the image intensity is thus

$$I(\boldsymbol{b}) = 1 - 2\sigma V_{\mathrm{p0}}(\boldsymbol{b})\otimes\mathrm{Im}[t_{\mathrm{obj}}(\boldsymbol{b})] + \sigma^2|V_{\mathrm{p0}}(\boldsymbol{b})\otimes t_{\mathrm{obj}}(\boldsymbol{b})|^2 + \sigma^2\langle|\Delta V_{\mathrm{p}}(\boldsymbol{b}, t)\otimes t_{\mathrm{obj}}(\boldsymbol{b})|^2\rangle_t, \tag{7d}$$

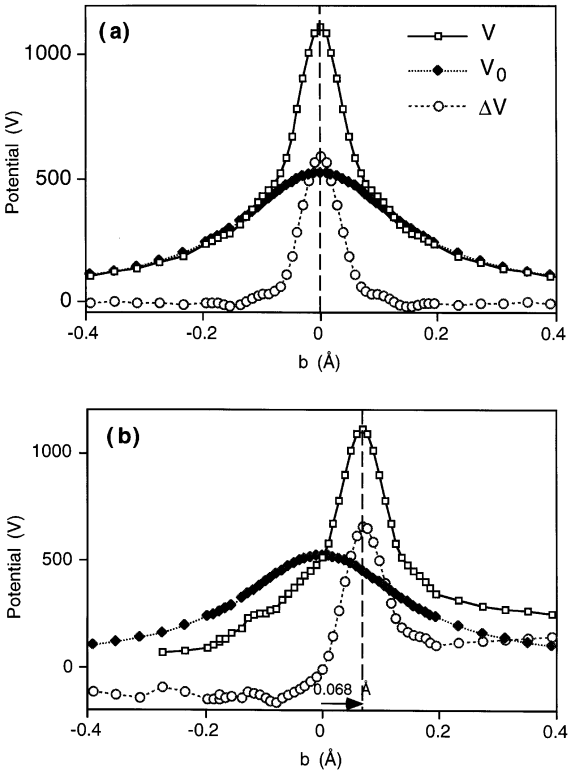

Fig. 2. Potential of a silicon atom with (V_0) and without (V) including the Debye–Waller factor. V is the instantaneous atomic potential and V_0 is the time-averaged atomic potential. The equilibrium position of the atom is $b = 0$. $\Delta V = V - V_0$ (dash-dotted line) is the deviation of the atomic potential from the time averaged potential V_0 when the atomic displacement is (a) $u_\kappa = 0$ or (b) $u_\kappa = 0.068$ Å. The arrowhead in (b) indicates the displacement of the atom. The mean square-root atom vibration amplitude was taken as 0.07 Å in the calculation.

where $\otimes$ indicates a convolution calculation, $t_{\mathrm{obj}}(x,y)$ characterizes the information transfer of the objective lens and it is a Fourier transform of the objective lens transfer function $T_{\mathrm{obj}}(\boldsymbol{u})$, and $\langle\ \rangle_t$ represents the time average of the image intensity. The first term is the incident beam, the second term is the interference between the center beam with the Bragg diffracted beams (the first-order effect), e.g., the bright-field lattice image, the third term is the interference between the Bragg reflected beams (the second-order effect), and the last term is the contribution made by TDS, a second-order effect. This equation clearly shows that *the contribution made by TDS is of the same order of magnitude as the cross interference term between Bragg beams excluding the central transmitted beam*, since ΔV is comparable with V_0 and it is peaked at the nuclear sites. On the image contrast, the second term (the bright field term) can produce contrast reversal as the lens defocus is changed, but the intensity contributed by TDS is always positive at the atom sites. Therefore, at the Schertzer defocus condition under which the atomic columns have dark contrast, adding the TDS contribution can reduce the darkness of the atom columns, resulting in a decrease in image contrast. This is the importance of TDS in HRTEM, and it can contribute some fine features more than the conventional understanding of "white noise".

Alternatively, atomic-scale contrast feature introduced by phonon scattered electrons can be understood based on the Z-contrast imaging in scanning transmission electron microscopy. With the use of a large angle

annular dark-field detector, atomic resolution, chemical sensitive Z-contrast image can be formed. The most striking feature of this type of image is that the atomic columns always show bright contrast (at least for perfect crystals) and there is no contrast reversal with a change in defocus, indicating that phonon scattering is a localized process. This type of large-angle phonon "absorption" contrast is due to the third term given in Eq. (7d), which is peaked at the atom sites and is positive at any defocus condition. The fine contrast introduced in atomic scale by TDS is determined primarily by the localization nature of phonon scattering, regardless if the atomic vibration is treated using the Debye model or the Einstein model with random phase approximation.

The question, however, is why the TDS is small in our experimentally observed diffraction pattern? Three reasons may account for this. First, the TDS intensity is distributed in the entire diffraction plane instead of accumulating at the reciprocal lattice points like the Bragg reflections. Secondly, TDS is incoherent, while Bragg reflections are coherent. The incoherence may give less intensity. Finally, TDS can scatter electrons into an angular range much larger than the objective aperture size or the column angle of an TEM, and it is usually believed that the electron backscattering is mainly produced by TDS. Therefore, most of the TDS are invisible in the experimentally observed diffraction pattern/image, but they do take away the intensity of the elastic wave. This could be one of the reasons why the observed electron intensity after being scattered by a thin crystal is always 5–15% smaller than the intensity of the incident beam [10]. More importantly, TDS is a very localized scattering process since ΔV is a much narrow function than V_0 (see Fig. 2), the intensity taken away by TDS comes from the nuclear positions of the atoms. With consideration of the strong zone-axis channeling effect in HRTEM [17], the contrast at the atom columns will be dramatically affected by TDS. Thus, it is believed that TDS could be responsible, at least in part, for the difference between the calculated image using pure elastic scattering theory and the experimentally observed image with the use of an energy filter. It is desirable to calculate the HRTEM image including the contribution made by multiple phonon scattering. This is the objective of the following sections.

4. The optical potential and its application for recovering multiple diffuse scattering

From the quantum mechanical transition theory, the transition out of the elastic state (or ground state) is characterized by a matrix element H_{n0}, and the transition back to the elastic state is by H_{0n}, and they are correlated by $H_{n0} = H_{0n}^*$. This means that the mechanism that determines the intensity loss of the elastic wave must be directly correlated to the intensity gaining process in the excited state, because the total scattering intensity of elastic and inelastic waves must be conserved. Therefore, the optical potential that represents the effect of inelastic excitation on the elastic wave could be applied, in principle, for recovering the multiple diffuse scattering process in a practical calculation. This is possible only if the total scattering governed by Eq. (5a) and (6) is conserved (see Appendix A for a theoretical proof).

To transform the physical argument above into mathematical expressions, we introduce a density matrix that can be applied conveniently for calculating either images or diffraction patterns

$$\rho(\boldsymbol{r}, \boldsymbol{r}') = \sum_{n=0} \Psi_n(\boldsymbol{r})\Psi_n^*(\boldsymbol{r}'), \tag{8}$$

where the sum of n is over all of the crystal states including the elastic scattering state (ground state). The electron diffraction pattern including TDS can be calculated by taking a double Fourier transform of the density matrix

$$I(\tau) = \int \mathrm{d}\boldsymbol{r} \int \mathrm{d}\boldsymbol{r}' \exp[-2\pi \mathrm{i}\boldsymbol{\tau}\cdot(\boldsymbol{r}-\boldsymbol{r}')]\rho(\boldsymbol{r}, \boldsymbol{r}'). \tag{9}$$

The intensity distribution in the electron image can be calculated by

$$I(\boldsymbol{r}) = \int \mathrm{d}\boldsymbol{r}_1 \int \mathrm{d}\boldsymbol{r}_2 \, \rho(\boldsymbol{r}_1, \boldsymbol{r}_2) t(\boldsymbol{r} - \boldsymbol{r}_1) t^*(\boldsymbol{r} - \boldsymbol{r}_2), \tag{10}$$

where $t(\boldsymbol{r})$ characterizes the information transfer property of the optical system in an electron microscope.

For the convenience of the discussion, we introduce a real space dynamic form factor defined by [18,19]

$$s(\boldsymbol{r}, \boldsymbol{r}_1) = \frac{1}{e^2} \sum_{m=1} H_{0m}(\boldsymbol{r}) H_{m0}(\boldsymbol{r}_1) = \int \mathrm{d}\boldsymbol{Q} \int \mathrm{d}\boldsymbol{Q}' \exp[2\pi \mathrm{i}(\boldsymbol{r} \cdot \boldsymbol{Q} - \boldsymbol{r}_1 \cdot \boldsymbol{Q}')] S(\boldsymbol{Q}, \boldsymbol{Q}'). \tag{11}$$

The calculation of $s(\boldsymbol{r}, \boldsymbol{r}_1)$ is given in Appendix B. Eq. (6) can be converted into an integral equation

$$\Psi_0(\boldsymbol{r}) = \Psi_0^{(0)}(\boldsymbol{r}) + e^2 \int \mathrm{d}\boldsymbol{r}_1 \, G(\boldsymbol{r}, \boldsymbol{r}_1) \int \mathrm{d}\boldsymbol{r}_2 \, G(\boldsymbol{r}_1, \boldsymbol{r}_2) s(\boldsymbol{r}_1, \boldsymbol{r}_2) \Psi_0(\boldsymbol{r}_2), \tag{12}$$

where $\Psi_0^{(0)}(\boldsymbol{r})$ is the elastic wave without the influence of the V' potential,

$$\left(-\frac{\hbar^2}{2m_0} \nabla^2 - eV_0 - E \right) \Psi_0^{(0)}(\boldsymbol{r}) = 0. \tag{13}$$

Eq. (12) can be solved iteratively

$$\begin{aligned} \Psi_0(\boldsymbol{r}) = \Psi_0^{(0)}(\boldsymbol{r}) &+ e^2 \int \mathrm{d}\boldsymbol{r}_1 \int \mathrm{d}\boldsymbol{r}_2 \, G(\boldsymbol{r}, \boldsymbol{r}_2) G(\boldsymbol{r}_1, \boldsymbol{r}_2) s(\boldsymbol{r}_1, \boldsymbol{r}_2) \Psi_0^{(0)} r(\boldsymbol{r}_2) \\ &+ e^4 \int \mathrm{d}\boldsymbol{r}_1 \int \mathrm{d}\boldsymbol{r}_2 \int \mathrm{d}\boldsymbol{r}_3 \int \mathrm{d}\boldsymbol{r}_4 \, G(\boldsymbol{r}, \boldsymbol{r}_1) G(\boldsymbol{r}_1, \boldsymbol{r}_2) G(\boldsymbol{r}_2, \boldsymbol{r}_3) G(\boldsymbol{r}_3, \boldsymbol{r}_4) s(\boldsymbol{r}_1, \boldsymbol{r}_2) s(\boldsymbol{r}_3, \boldsymbol{r}_4) \Psi_0^{(0)}(\boldsymbol{r}_4) + \ \ldots \end{aligned} \tag{14}$$

Substituting Eqs. (12) and (5b) into Eq. (8) yields

$$\rho(\boldsymbol{r}, \boldsymbol{r}') = \Psi_0(\boldsymbol{r}) \Psi_0^*(\boldsymbol{r}') + e^2 \int \mathrm{d}\boldsymbol{r}_1 \int \mathrm{d}\boldsymbol{r}_2 \, G(\boldsymbol{r}, \boldsymbol{r}_1) G^*(\boldsymbol{r}', \boldsymbol{r}_2) s(\boldsymbol{r}_1, \boldsymbol{r}_2) \psi_0(\boldsymbol{r}_1) \Psi_0^*(\boldsymbol{r}_2)]. \tag{15}$$

From the proof given in Appendix C, a substitution of Eq. (14) into Eq. (15) recovers all the orders of diffuse scattering terms. Therefore, *by inclusion of the optical potential in the dynamical calculation of the elastic wave* [Eq. (6)], *the high-order diffuse scattering are fully recovered in the calculations made using the equation for the first-order diffuse scattering* [Eq. (5a)], *and more importantly, the incoherence in phonon excitation is considered properly*. This conclusion agrees completely with that obtained previously based on the "frozen" lattice model for TDS and the system containing short-range point defects such as oxygen vacancies [20,21]. This is a rather important conclusion which establishes the basis for generalizing the existing first-order scattering theories for calculating high-order diffuse scattering. *The density matrix theory is unique to treat the incoherence between different orders of diffuse scattering.*

In conventional dynamical diffraction, inclusion of Debye–Waller factor and the optical potential accounts only for the effect of diffuse scattering on the elastic wave. This task is included in the first term at the right-hand side of Eq. (15), the elastic wave component. The calculations result in Bragg reflections. One must perform the calculation of the second term in order to include the contributions made by the diffusely scattered electrons.

We now come back to the question raised at the end of Section 2: what is missing if Green's function is replaced by its form in free space? In Eq. (15), the $\Psi_0(\boldsymbol{r}_1)$ function is responsible for exciting the diffuse scattering at $\boldsymbol{r}_1$, the $\Psi_0(\boldsymbol{r}_2)$ function is responsible for exciting the diffuse scattering at $\boldsymbol{r}_2$, while the strength of the excitation is determined by a "probability" and spatial correlation (or coherence) function $s(\boldsymbol{r}_1, \boldsymbol{r}_2)$. The dynamic diffraction of the inelastic wave from its emission point $\boldsymbol{r}_1$ to the observation point $\boldsymbol{r}$ is characterized

by Green's function $G(\boldsymbol{r}, \boldsymbol{r}_1)$. If $G(\boldsymbol{r}, \boldsymbol{r}_1)$ is replaced by its form in free-space, it means that the subsequent dynamical diffraction of the emitted inelastic wave is ignored, while the multiple diffuse scattering is still preserved. In other words, the calculation covers the dynamic diffraction before the first inelastic event and the multiple inelastic scattering but not Bragg reflections after and between the inelastic events. This is the consequence of the Yoshioka's approximation. Unfortunately, this approximation has rarely been re-examined since it was proposed in 1957, and many calculations were performed with the inclusion of the optical potential, but the consequence and real nature of the optical potential were ambiguous. It is hoped that this paper will clear it up.

5. Calculation under the small angle scattering approximation

In a practical calculation, one of the keys is to solve Eq. (6). The first step is to find Green's function. For a general case Green's function has been given by Dudarev et al. [22] and Wang [23], but the general solution involves a huge amount of computation and it simply becomes impractical. In this section, we introduce an approximated form of Green's function for high-energy electron under the small angle scattering approximation, which can be reasonably computed in practice.

We consider the first-order inelastic scattering equation as a start:

$$\left[-\frac{\hbar^2}{2m_0}\nabla^2 - eV_0 - E) \right]\Psi_n = -H_{n0}\Psi_0, \tag{16a}$$

which can be converted into an integral equation with the use of Green's function

$$\Psi_n(\boldsymbol{r}) = -\int \mathrm{d}\boldsymbol{r}_1\, G(\boldsymbol{r}, \boldsymbol{r}_1) H_{n0}(\boldsymbol{r}_1)\Psi_0(\boldsymbol{r}_1). \tag{16b}$$

Alternatively, Eq. (16b) can be directly obtained from Eq. (5a) using the real-space multislice theory, which was initiated by Van Dyck [24] and has lately been developed by Chen et al. [25–27]. Fig. 3 shows a schematic diagram of a thin foil in TEM, where the incident beam strikes the surface at a small angle. The

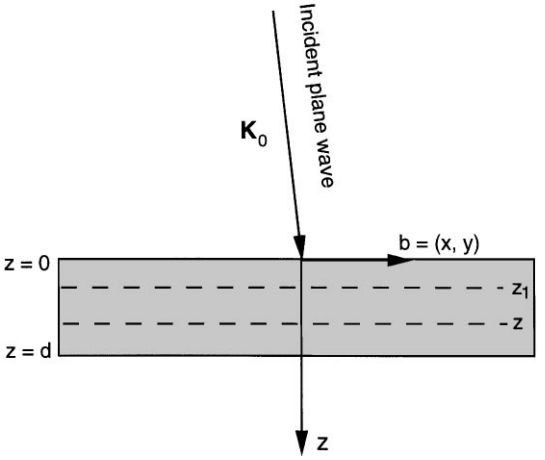

Fig. 3. A model illustrating transmission electron scattering in a thin foil of uniform thickness and the corresponding coordination selection used for the theoretical description.

z-axis is chosen downward normal to the specimen surface. If the wave function is written in a form $\Psi(\boldsymbol{r}) = \exp(2\pi i \boldsymbol{K}_0 \cdot \boldsymbol{r})\Phi(\boldsymbol{r})$, where $\boldsymbol{K}_0$ is the wave vector of the incident beam, the $\partial^2\Phi/\partial z^2$ term can be dropped under the small-angle scattering approximation Hence

$$\frac{\partial \Phi_n(\boldsymbol{r})}{\partial_z} \approx \varsigma\left[\Xi + \frac{2m_0}{\hbar^2} eV_0\right]\Phi_n(\boldsymbol{r}) - \frac{2m_0}{\hbar^2} H_{n0}(\boldsymbol{r})\Phi_0(\boldsymbol{r}) \tag{17a}$$

where $\varsigma = i/4\pi K_{0z}$,

$$\Xi = \frac{\partial^2}{\partial x^2} + \frac{\partial^2}{\partial y^2} + 4\pi i\left(K_{0x}\frac{\partial}{\partial y} + K_{0y}\frac{\partial}{\partial y}\right) \tag{17b}$$

is an operator, and $\boldsymbol{b} = (x, y)$ is the coordinate in the image plane. For practical HRTEM dominated by the reflections in the zero-order Laue zone, the crystal potential V_0 is effectively independent of z. Thus the projected potential approximation holds. The solution of Eq. (17a) can be written in the form

$$\Phi_n(\boldsymbol{r}) = \xi\int_0^z \mathrm{d}z'\, O_p(\boldsymbol{b}, z - z')[H_{n0}(\boldsymbol{b}, z')\Phi_0(\boldsymbol{b}, z')], \tag{18a}$$

where the operator O_p is defined as

$$O_p(\boldsymbol{b}, z - z_1) = \exp\left\{\varsigma\left[\Xi + \frac{2m_0}{\hbar^2} eV_0\right](z - z_1)\right\}, \tag{18b}$$

and $\xi = -(2m_0/\hbar^2)\varsigma$. The operator O_p represents the consecutive phase grating and Fresnel propagation calculations in the multislice theory [24].

To match the form of Eq. (16b), we add the plane wave component back to Eq. (18a) and perform the following calculation using an identity:

$$\int \mathrm{d}\boldsymbol{r}_1\, \delta(\boldsymbol{b} - \boldsymbol{b}_1)\,\delta(z_1 - z')H_{n0}(\boldsymbol{b}_1, z_1)\Phi_0(\boldsymbol{b}_1, z_1) = H_{n0}(\boldsymbol{b}, z')\Phi_0(\boldsymbol{b}, z'), \tag{19}$$

$$\begin{aligned}\Psi_n(\boldsymbol{r}) &= \exp(2\pi i \boldsymbol{K}_0 \cdot \boldsymbol{r})\xi\int_0^z \mathrm{d}z'\, O_p(\boldsymbol{b}, z - z')\left[\int \mathrm{d}\boldsymbol{r}_1\, \delta(\boldsymbol{b} - \boldsymbol{b}_1)\delta(z_1 - z')H_{n0}(\boldsymbol{r}_1)\exp(-2\pi i \boldsymbol{K}_0 \cdot \boldsymbol{r}_1)\Psi_0(\boldsymbol{r}_1)\right] \\ &= \xi\exp(2\pi i \boldsymbol{K}_0 \cdot \boldsymbol{r})\int \mathrm{d}\boldsymbol{r}_1\, O_p(\boldsymbol{b}, z - z_1)[\delta(\boldsymbol{b} - \boldsymbol{b}_1)]\exp(-2\pi i \boldsymbol{K}_0 \cdot \boldsymbol{r}_1)H_{n0}(\boldsymbol{r}_1)\Psi_0(\boldsymbol{r}_1).\end{aligned} \tag{20}$$

A comparison of Eq. (20) with Eq. (16b) gives Green's function

$$\begin{aligned}G(\boldsymbol{r}, \boldsymbol{r}_1) &\approx -\xi\exp[2\pi i \boldsymbol{K}_0 \cdot (\boldsymbol{r} - \boldsymbol{r}_1)]O_p(\boldsymbol{b}, z - z_1)[\delta(\boldsymbol{b} - \boldsymbol{b}_1)] \\ &= -\xi\exp[2\pi i \boldsymbol{K}_0 \cdot (\boldsymbol{r} - \boldsymbol{r}_1)]\int_0^z \mathrm{d}z'\, O_p(\boldsymbol{b}, z - z')\{\delta(\boldsymbol{b} - \boldsymbol{b}_1)\delta(z' - z_1)\}, \quad \text{for } z > z_1.\end{aligned} \tag{21}$$

It can be proved that this Greens function satisfies Eq. (5c) under the small angle scattering approximation (See Appendix D). The accurate solution of Green's function is independent of $\boldsymbol{K}_0$ [22,23]. The scattering from a point source should be more symmetric. On the other hand, our observation is only at the small angle range, the waves scattered to high angles are unlikely to contribute to the image formed by lower angle Bragg reflections (see Fig. 4). Thus, the part of Green's function with appreciable contribution to the observed wave

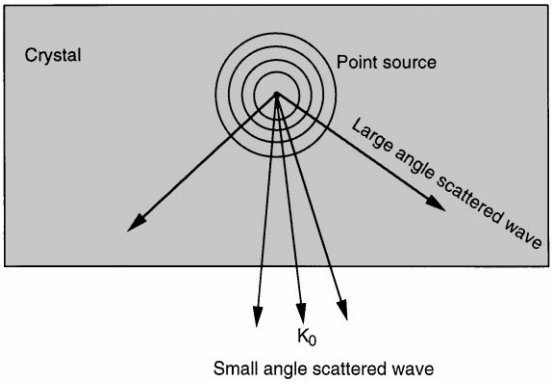

Fig. 4. A schematic model showing the spherical wave emitted from a point source in the crystal and the small angles components near $\boldsymbol{K}_0$ that are likely to contribute to the observed image/diffraction pattern in TEM. The waves distributed at high angle range make little contribution to the observed image if the back scattering is ignored for high-energy electrons.

is confined within the nearby region of the incident beam $\boldsymbol{K}_0$. This is likely to be the reason for Green's function given in Eq. (21) to depend on the incident beam direction under the small angle approximation. A substitution of Eq. (21) into Eq. (15) leads to

$$\begin{aligned}\rho(\boldsymbol{r},\boldsymbol{r}') &= \Psi_0(\boldsymbol{r})\Psi_0^*(\boldsymbol{r}') + e^2\xi^2\int \mathrm{d}\boldsymbol{Q}\int \mathrm{d}\boldsymbol{Q}'\, S(\boldsymbol{Q},\boldsymbol{Q}')\int \mathrm{d}\boldsymbol{r}_1\int \mathrm{d}\boldsymbol{r}_2\, \exp[2\pi \mathrm{i}\boldsymbol{r}_1\cdot\boldsymbol{Q}]\\ &\quad\times\exp[-2\pi\mathrm{i}\boldsymbol{r}_2\cdot\boldsymbol{Q}']\exp[2\pi\mathrm{i}\boldsymbol{K}_0\cdot(\boldsymbol{r}-\boldsymbol{r}')]\int_0^z \mathrm{d}z'\, O_p(\boldsymbol{b},z-z')\{\delta(\boldsymbol{b}-\boldsymbol{b}_1)\delta(z'-z_1)\}\\ &\quad\times\int_0^z \mathrm{d}z''\, O_p^*(\boldsymbol{b}',z'-z'')\{\delta(\boldsymbol{b}'-\boldsymbol{b}_2)\delta(z''-z_2)\}\Phi_0(\boldsymbol{r}_1)\Phi_0^*(\boldsymbol{r}_2)\\ &= \Psi_0(\boldsymbol{r})\Psi_0^*(\boldsymbol{r}') + e^2\xi^2\int \mathrm{d}\boldsymbol{Q}\int \mathrm{d}\boldsymbol{Q}'[S(\boldsymbol{Q},\boldsymbol{Q}')\\ &\quad\times\int_0^z \mathrm{d}z'\{O_p(\boldsymbol{b},z-z')[\exp[2\pi\mathrm{i}(\boldsymbol{b}\cdot\boldsymbol{Q}_b+z'Q_z)]\Phi_0(\boldsymbol{b},z')]\}\\ &\quad\times\int_0^z \mathrm{d}z''\{O_p^*(\boldsymbol{b}',z-z'')[\exp[-2\pi\mathrm{i}(\boldsymbol{b}'\cdot\boldsymbol{Q}_b'+z''Q_z')]\Phi_0^*(\boldsymbol{b}',z'')]\}]\\ &= \Psi_0(\boldsymbol{r})\Psi_0^*(\boldsymbol{r}') + e^2\xi^2\int \mathrm{d}\boldsymbol{Q}\int \mathrm{d}\boldsymbol{Q}'\, S(\boldsymbol{Q},\boldsymbol{Q}')\psi(\boldsymbol{Q},\boldsymbol{b},z)\psi^*(\boldsymbol{Q}',\boldsymbol{b}',z). \end{aligned}\tag{22a}$$

where

$$\psi(\boldsymbol{Q},\boldsymbol{b},z) = \int_0^z \mathrm{d}z'\,\{O_p(\boldsymbol{b},z-z')[\exp[2\pi\mathrm{i}(\boldsymbol{b}\cdot\boldsymbol{Q}_b+z'Q_z)]\Phi_0(\boldsymbol{b},z')]\}.\tag{22b}$$

The physical meaning of Eq. (22a) can be given as follows. At point $(\boldsymbol{b},z')$ in the specimen, the initial source of intensity is the elastic wave $\Phi_0(\boldsymbol{b},z')$. The effect of momentum transfer $\hbar\boldsymbol{Q}$ in the inelastic scattering is equivalent to multiplying a plane wave component of $\exp[2\pi\mathrm{i}(\boldsymbol{b}\cdot\boldsymbol{Q}_b+z'Q_z)]$ onto the elastic wave $\Phi_0(\boldsymbol{b},z')$, whose propagation from $(\boldsymbol{b},z')$ to $(\boldsymbol{b},z)$ must suffer from dynamical elastic diffraction characterized by the

$O_p(\boldsymbol{b}, z - z')$ operator. The wave $\psi(\boldsymbol{Q}, \boldsymbol{b}, z)$ with momentum transfer $\hbar\boldsymbol{Q}$ observed at $(\boldsymbol{b}, z)$ is a sum of the waves generated from the crystal entrance face $z = 0$ to $z = z$. For the total scattering intensity, on the other hand, the probability for generating the wave with momentum transfer $\hbar\boldsymbol{Q}$ is determined by the dynamic form factor $S(\boldsymbol{Q}, \boldsymbol{Q}')$, thus, the intensity of the diffuse scattering wave is $S(\boldsymbol{Q}, \boldsymbol{Q}')\psi(\boldsymbol{Q}, \boldsymbol{b}, z)\psi^*(\boldsymbol{Q}', \boldsymbol{b}', z)$, and the total intensity is an integration over the entire space of momentum transfer.

6. The Bloch wave–multislice approach

The non-local property of the optical potential is essentially important in recovering the high-order diffuse scattering. The introduction of a non-local potential V' in the equation makes it difficult to be solved using the conventional multislice approach, although it can be done in principle [28]. In this case, the Bloch wave theory is likely to be the most suitable choice. Since the average structure is described by a periodic potential V_0, the Bloch wave theory is adequate to calculate Ψ_0, the elastic scattered wave is a linear superposition of Bloch waves $B_i(\boldsymbol{K}_0, \boldsymbol{r})$ [29],

$$\Psi_0(\boldsymbol{r}) = \sum_i \alpha_i(\boldsymbol{K}_0) B_i(\boldsymbol{K}_0, \boldsymbol{r}), \tag{23a}$$

and $B_i(\boldsymbol{K}_0, \boldsymbol{r})$ is the ith eigensolution of Eq. (6),

$$B_i(\boldsymbol{K}, \boldsymbol{r}) = \sum_g C_g^{(i)}(\boldsymbol{K}) \exp[2\pi\mathrm{i}(\boldsymbol{K} + \boldsymbol{g})\cdot\boldsymbol{r} + 2\pi\mathrm{i}v_i z]. \tag{23b}$$

where $\alpha_i(\boldsymbol{K}) = C_{I_o}^{(i)}\boldsymbol{K}_0$ are the superposition coefficients, $C_{I0}^{(i)}(\boldsymbol{K}_0)$ are the elements of the first column of the inverse of the matrix whose elements are $C_g^{(i)}$ (row i and column g). The coefficients $C_g^{(i)}(\boldsymbol{K})$ and eigenvalue v_i are determined by an eigen equation in the Bloch wave theory. Substituting Eq. (23b) into Eq. (6) and using the inverse Fourier transform, a set of coupled algebraic equations are obtained

$$[K^2 - (\boldsymbol{K} + v_i z + \boldsymbol{g})^2]C_g^{(i)} + \frac{2m_0 e}{h^2}\sum_h [V_{g-h} + V'^{(i)}_{gh}]C_h^{(i)} = 0, \tag{24}$$

where V_g are the Fourier coefficients of the crystal potential and those of the complex potential V' are

$$V'^{(i)}_{gh} = \frac{e}{V_c}\int \mathrm{d}\boldsymbol{Q}\int \mathrm{d}\boldsymbol{Q}'\, S(\boldsymbol{Q}, \boldsymbol{Q}')\hat{G}(\boldsymbol{k}_i + \boldsymbol{g} - \boldsymbol{Q}, \boldsymbol{Q}' - \boldsymbol{k}_i - \boldsymbol{h}), \tag{25}$$

V_c is the volume of the crystal, and $\hat{G}(\boldsymbol{U}, \boldsymbol{V})$ is the double Fourier transform of $G(\boldsymbol{r}, \boldsymbol{r}_1)$, to be calculated below. For a periodically structured crystal and in the Einstein model [18],

$$S(\boldsymbol{Q}, \boldsymbol{Q}') = \sum_{g''}\delta(\boldsymbol{Q}' - \boldsymbol{Q} - \boldsymbol{g}'')\Bigg\{\sum_\beta \exp[2\pi\mathrm{i}\boldsymbol{r}(\beta)\cdot\boldsymbol{g}'']f_\beta^e(\boldsymbol{Q})[f_\beta^e(\boldsymbol{Q} + \boldsymbol{g}'')]^* \times\{\exp[-W_\beta(\boldsymbol{g}'')] - \exp[-W_\beta(\boldsymbol{Q}) - W_\beta(\boldsymbol{Q} + \boldsymbol{g}'')]\Bigg\}, \tag{26}$$

where the sum of β is over all the atoms in the unit cell, and $\boldsymbol{g}''$ are the reciprocal lattice vectors. Eq. (25) can be simplified accordingly

$$V'^{(i)}_{gh} = \frac{e}{V_c}\sum_{g''}\int \mathrm{d}\boldsymbol{Q}\, S(\boldsymbol{Q}, \boldsymbol{Q} + \boldsymbol{g}'')\hat{G}(\boldsymbol{k}_i + \boldsymbol{g} - \boldsymbol{Q}, \boldsymbol{Q} + \boldsymbol{g}'' - \boldsymbol{k}_i - \boldsymbol{h}). \tag{27}$$

A general method has been proposed based on the Born series for the calculation of $V'^{(i)}_{gh}$ [23]. The amount for calculating $\hat{G}(\boldsymbol{U},\boldsymbol{V})$ is usually large, but this calculation is needed only for the reciprocal space in which the mixed dynamic form factor $S(\boldsymbol{Q}, \boldsymbol{Q} + \boldsymbol{g}'')$ is appreciable.

Eq. (24) can be solved numerically using the FORTRAN source code developed by Spence and Zuo [1]. If $\hat{G}(\boldsymbol{U}, \boldsymbol{V})$ is known, the mixed dynamic form factor is also known for phonon excitation (see Appendix A), the optical potential can be calculated. We now use Green's function given in Eq. (21) to calculate $\hat{G}(\boldsymbol{U}, \boldsymbol{V})$. From an identity of

$$\delta(\boldsymbol{b} - \boldsymbol{b}_1) = \int \mathrm{d}\tau_b \exp[2\pi \mathrm{i} \boldsymbol{\tau}_b \cdot (\boldsymbol{b} - \boldsymbol{b}_1)],$$

one has

$$\begin{aligned}\hat{G}(\boldsymbol{U}, \boldsymbol{V}) &= -\xi \int \mathrm{d}\boldsymbol{r} \int \mathrm{d}\boldsymbol{r}_1 \exp[-2\pi \mathrm{i}(\boldsymbol{U} - \boldsymbol{K}_0)\cdot \boldsymbol{r}] \exp[-2\pi \mathrm{i}(\boldsymbol{V} - \boldsymbol{K}_0)\cdot \boldsymbol{r}_1] O_p(\boldsymbol{b}, z - z_1)[\delta(\boldsymbol{b} - \boldsymbol{b}_1)] \\ &= -\xi \int \mathrm{d}\boldsymbol{r} \exp[-2\pi \mathrm{i}(\boldsymbol{U} - \boldsymbol{K}_0)\cdot \boldsymbol{r}] \Bigg[\int \mathrm{d}z_1 \exp[-2\pi \mathrm{i}(V_z - K_{0z})\cdot z_1] \\ &\quad \times O_p(\boldsymbol{b}, z - z_1)\{\exp[2\pi \mathrm{i}(\boldsymbol{V}_b - \boldsymbol{K}_{0b})\cdot \boldsymbol{b}]\} \Bigg], \end{aligned} \tag{28}$$

where $O_p(\boldsymbol{b}, z - z_1)[\exp(2\pi \mathrm{i}(\boldsymbol{V}_b - \boldsymbol{K}_{0b})\cdot \boldsymbol{b})]$ is the real space multislice calculation of the incident wave, $\exp[2\pi \mathrm{i}(\boldsymbol{V}_b - \boldsymbol{K}_{0b})\cdot \boldsymbol{b}]$, from thickness $z = z_1$ to $z = z$ (for $z > z_1$ in forward scattering) [30,31], and the integration of z_1 is to sum the contributions of the waves generated from different crystal thicknesses. The combination of the Bloch wave and multislice theory is likely to solve Eq. (24). The small angle forward scattering approximation illustrated in Fig. 4 is the key for computing Green's function using the multislice theory.

This section clearly shows that the optical potential has a specific form and it must be computed precisely for both real and imaginary parts, in order to be correctly applied to recover the high order diffuse scattering.

7. The real component of the optical potential

The optical potential is generally a complex function. Its imaginary component accounts for the absorption effect of the elastic wave. Its real component represents the return scattering of the inelastic wave back to the elastic wave, or so called "virtual" inelastic scattering process [32,33]. To illustrate this point, one uses the Yoshioka's approximation by replacing Green's function with its form in free space, which means there is no atom scattering after inelastic excitation. The double Fourier transform of the free space Green's function is

$$\hat{G}_0(\boldsymbol{U}, \boldsymbol{V}) = \frac{m_0}{2\pi^2 \hbar^2} \lim_{\varepsilon \to 0} \frac{\delta(\boldsymbol{U} + \boldsymbol{V})}{(U^2 - K_0^2 - \mathrm{i}\varepsilon)}, \tag{29}$$

thus, the matrix elements of the optical potential are

$$V'^{(i)}_{gh} \approx \frac{e\gamma m_0}{2\pi^2 \hbar^2 V_c} \left[\int \mathrm{d}\tau(\boldsymbol{U}) \frac{S(\boldsymbol{k}_i + \boldsymbol{g} - \boldsymbol{U},\ \boldsymbol{k}_i + \boldsymbol{h} - \boldsymbol{U})}{U^2 - K0^2} + \mathrm{i} \frac{\pi}{2K_0} \int \mathrm{d}\sigma(\boldsymbol{U})\, S(\boldsymbol{k}_i + \boldsymbol{g} - \boldsymbol{U}, \boldsymbol{k}_i + \boldsymbol{h} - \boldsymbol{U}) \right], \tag{30}$$

where the integral $\tau(\boldsymbol{U})$ is over the entire reciprocal space except a spherical shell defined by $|\boldsymbol{U}| = K_0$; the integral $\sigma(\boldsymbol{U})$ is over the Ewald sphere surface defined by $|\boldsymbol{U}| = K_0$. Eq. (30) is the most familiar form of the absorption potential usually introduced in dynamical calculations. The imaginary part is the result of an integral over the scattering falling on the surface of the Ewald sphere, the scattering that satisfies the conservation of energy, which is allowed in practice and can occur. On the other hand, the volume integral in the real component covers the entire reciprocal space except the surface of the Ewald sphere, thus, the scattering does not satisfy the conservation of energy and is unlikely to occur. Thus, the virtually scattered

wave will return to the elastic wave, but with a phase modulation. Therefore, it can be simply understood that the imaginary component characterizes the lost in intensity, while the real component signifies the gain in elastic wave intensity. There are numerous techniques developed to calculate the imaginary part of Eq. (30) [34–38]. The real component has, however, always been ignored because it is much smaller than the crystal potential, but it should have the same magnitude as the imaginary component. It is necessary to re-compute the real part and table it as for the imaginary part!

We have proved in Section 4 that a full inclusion of the optical potential in the calculation can recover the multiple diffuse scattering in the calculation made for the first-order scattering. This recovery process is required to meet three conditions: first the real component of the optical potential must be included in the calculation; second Green's function cannot be replaced by its form in free space; and third, the non-local property of the optical potential needs to be retained.

Most of the current calculations reported in the literature were performed considering only the imaginary part of the optical potential given in Eq. (30). Two effects are missing in these calculations: one, the virtual inelastic scattering is dropped, and the other, the dynamic diffraction after the inelastic scattering is ignored, while the multiple inelastic scattering is still preserved.

8. A summary of the computation procedures

Our entire derivations are based on Eq. (6) and (15),

$$\left[\left(-\frac{\hbar^2}{2m_0}\nabla^2 - eV_0 - E\right)\right]\Psi_0(\boldsymbol{r}) = e^2\int \mathrm{d}\boldsymbol{r}_1\, G(\boldsymbol{r},\boldsymbol{r}_1)s(\boldsymbol{r},\boldsymbol{r}_1)\Psi_0(\boldsymbol{r}_1), \tag{31a}$$

$$\rho(\boldsymbol{r},\boldsymbol{r}') = \Psi_0(\boldsymbol{r})\Psi_0^*(\boldsymbol{r}') + e^2\int \mathrm{d}\boldsymbol{r}_1\int \mathrm{d}\boldsymbol{r}_2\, G(\boldsymbol{r},\boldsymbol{r}_1)G^*(\boldsymbol{r}',\boldsymbol{r}_2)s(\boldsymbol{r}_1,\boldsymbol{r}_2)\Psi_0(\boldsymbol{r}_1)\Psi_0^*(\boldsymbol{r}_2) \tag{31b}$$

which were derived under the ground-state approximation. The major task is to calculate Green's function and solving Eq. (31a). As a summary, the main procedures for calculating the image/diffraction pattern of the multiple-elastically and multiple-phonon scattered (or thermal diffusely scattered) electrons, with the consideration of the incoherence among phonon excitations, can be summarized as below.

1. For a given crystal structure, compute the Fourier transform of Green's function using the multislice theory:

$$\hat{G}(\boldsymbol{U},\boldsymbol{V}) = -\xi\int \mathrm{d}\boldsymbol{r}\exp[-2\pi\mathrm{i}(\boldsymbol{U}-\boldsymbol{K}_0)\cdot\boldsymbol{r}]\left[\int \mathrm{d}z_1\exp[-2\pi\mathrm{i}(V_z - K_{0z})\cdot z_1]\right.$$
$$\left.\times\, O_p(\boldsymbol{b}, z-z_1)\{\exp[2\pi\mathrm{i}(\boldsymbol{V}_b - \boldsymbol{K}_{0b})\cdot\boldsymbol{b}]\}\right], \tag{32}$$

   where the small-angle-scattering approximation (or high-energy approximation) and the projected potential approximation (for zero-order Laue zone) were made.
2. Calculate the matrix elements of the optical potential

$$V'^{(i)}_{gh} = \frac{e}{V_c}\int \mathrm{d}\boldsymbol{Q}\int \mathrm{d}\boldsymbol{Q}'\, S(\boldsymbol{Q},\boldsymbol{Q}')\hat{G}(\boldsymbol{k}_i + \boldsymbol{g} - \boldsymbol{Q}, \boldsymbol{Q}' - \boldsymbol{k}_i - \boldsymbol{h}). \tag{33}$$

   The Einstein model is optional for this step in order to expedite the calculation.
3. Solve the eigenvalue equation for the Bloch wave coefficients $C_g^{(i)}(\boldsymbol{K})$, and obtain the elastically scattered wave $\Phi_0(\boldsymbol{r})$

4. Calculate the total amplitude function for an inelastic scattering with momentum transfer $\hbar\boldsymbol{Q}$ generated in the entire thickness of the crystal using the multislice theory

$$\psi(\boldsymbol{Q}, \boldsymbol{b}, z) = \int_0^z \mathrm{d}z_1\{O_p(\boldsymbol{b}, z - z_1)[\exp[2\pi\mathrm{i}(\boldsymbol{b}\cdot\boldsymbol{Q}_b + z_1 Q_z)]\Phi_0(\boldsymbol{b},z_1)]\}, \tag{34}$$

5. Compute the density matrix

$$\rho(\boldsymbol{r}, \boldsymbol{r}') = \Phi_0(\boldsymbol{r})\Phi_0^*(\boldsymbol{r}') + e^2\xi^2 \int\mathrm{d}\boldsymbol{Q}\int\mathrm{d}\boldsymbol{Q}'\, S(\boldsymbol{Q}, \boldsymbol{Q}')\psi(\boldsymbol{Q}, \boldsymbol{b}, z)\psi^*(\boldsymbol{Q}', \boldsymbol{b}', z), \tag{35}$$

6. Compute the image/diffraction pattern from $\rho(\boldsymbol{r}, \boldsymbol{r}')$.

9. Conclusion

1. The "absorption" potential, or the optical potential in general, introduced first by Yoshioka is revisited. The approximation of replacing Green's function by its form in free-space is the root of dropping the multiple dynamic thermal diffuse scattering. Using Green's function for a crystal instead of its form in free space, a rigorous theoretical proof is given to show that the inclusion of the optical potential in the dynamical calculation automatically recovers the contributions made by the high-order diffuse scattering although the calculation is done using the equation derived for single diffuse scattering. The conclusion gives the basis for generalizing the conventional diffraction theories developed under the first-order diffuse scattering to cases where the specimen thickness is large and/or the degree of disorder is high. This conclusion agrees completely with the results derived previously based on the Frozen lattice model [20,21].
2. The optical potential is no longer a simple potential function, instead it is a non-local function strongly dependent on the dynamic diffraction in the crystal because of the involvement of the Green's function. It has a much richer meaning than the conventional interpretation of an absorption effect. These characteristics can be properly taken into account using a Bloch wave–multislice approach, in which the non-local effect is resolved in the Bloch wave matrix diagonalization and the dynamical effect is taken care using Green's function calculated by the multislice theory under the small-angle (or high-energy) approximation. It has also been emphasized that the real component of the potential, which has been ignored in most of the calculations, needs to be reconsidered because it has the same magnitude and function as the imaginary component.
3. Under the ground-state approximation, by which we mean that the crystal is in its ground state before each and every inelastic excitation, the introduction of the mixed dynamic form factor and the density matrix automatically produces the incoherence between different orders and different phonon excitation processes, resolving a big problem encountered by many theories, such as the "frozen" lattice model in which the quasi-elastic coherent scattering is a concern.
4. It is suggested that multiple thermal diffuse scattering (or phonon excitations) is likely to be the dominant source affecting image contrast in quantitative electron microscopy because phonon excitation is a very localized scattering process. To consider this effect properly in HRTEM image calculation, the theory proposed here or the one reported in Ref. [14] is adequate.
5. In the conventional dynamical calculation for the elastic wave, the Debye–Waller factor and the optical potential must be included to account for the effects of the phonon excitation on the elastic wave. This type of calculation, however, has missed the contribution from the phonon scattered electrons. The Debye–Waller factor accounts only for the reduction in Bragg reflected intensity due to atom vibration and it by no means has considered the contribution made by the TDS electrons.

Acknowledgements

Thanks to Prof. D. Van Dyck and Dr. J.H. Chen for stimulating discussions about the importance of phonon scattering in HRTEM. This research was supported by the Georgia Tech faculty development program (1997).

Appendix A

The numerical calculation is based on Eqs. (5a) and (6), which are

$$\left[\left(-\frac{\hbar^2}{2m_0}\nabla^2 - eV_0 - E\right)\right]\Psi_n \approx -H_{n0}\Psi_0, \tag{A.1}$$

or in the integral form

$$\Psi_n(\boldsymbol{r}) = -\int \mathrm{d}\boldsymbol{r}_1\, G(\boldsymbol{r},\boldsymbol{r}_1)H_{n0}(\boldsymbol{r}_1)\Psi_0(\boldsymbol{r}_1), \tag{A.2}$$

and

$$\left[\left(-\frac{\hbar^2}{2m_0}\nabla^2 - eV_0 - E\right)\right]\Psi_0(\boldsymbol{r}) = e^2\int \mathrm{d}\boldsymbol{r}_1\, G(\boldsymbol{r},\boldsymbol{r}_1)s(\boldsymbol{r},\boldsymbol{r}_1)\Psi_0(\boldsymbol{r}_1). \tag{A.3}$$

The conservation of total scattering intensity is proved using the current density defined in quantum mechanics

$$\int_\Sigma \mathrm{d}\boldsymbol{S}\cdot\boldsymbol{j} = \frac{\hbar}{2im_0}\int_{\mathrm{vol}} \mathrm{d}\boldsymbol{r}\sum_{n=0}[\Psi_n^*\nabla^2\Psi_n - \Psi_n\nabla^2\Psi_n^*], \tag{A.4}$$

where the integral is over the crystal volume. From Eq. (A.1) and using Eq. (A.2)

$$\begin{aligned}\sum_{n=1}[\Psi_n^*\nabla^2\Psi_n - \Psi_n\nabla^2\Psi_n^*] &= \frac{2m_0}{\hbar^2}\sum_{n=1}[\Psi_n^*H_{n0}\Psi_0 - \Psi_nH_{n0}^*\Psi_0^*]\\ &= -\frac{2m_0}{\hbar^2}\sum_{n=1}\left[\int \mathrm{d}\boldsymbol{r}_1\, G^*(\boldsymbol{r},\boldsymbol{r}_1)H_{n0}^*(\boldsymbol{r}_1)\Psi_0(\boldsymbol{r}_1)H_{n0}(\boldsymbol{r})\Psi_0(\boldsymbol{r})\right.\\ &\quad\left.-\int \mathrm{d}\boldsymbol{r}_1\, G(\boldsymbol{r},\boldsymbol{r}_1)H_{n0}(\boldsymbol{r}_1)\Psi_0(\boldsymbol{r}_1)H_{n0}^*(\boldsymbol{r})\Psi_0^*(\boldsymbol{r})\right]\\ &= -e^2\frac{2m_0}{\hbar^2}\left[\int \mathrm{d}\boldsymbol{r}_1\, G^*(\boldsymbol{r},\boldsymbol{r}_1)s^*(\boldsymbol{r},\boldsymbol{r}_1)\Psi_0(\boldsymbol{r}_1)\Psi_0(\boldsymbol{r}) - \int \mathrm{d}\boldsymbol{r}_1\, G(\boldsymbol{r},\boldsymbol{r}_1)s(\boldsymbol{r},\boldsymbol{r}_1)\psi_0(\boldsymbol{r}_1)\Psi_0^*(\boldsymbol{r})\right]\\ &= -e\frac{2m_0}{\hbar^2}\{[V'\Psi_0(\boldsymbol{r})]^*\psi_0(\boldsymbol{r}) - [V'\Psi_0(\boldsymbol{r})]\Psi_0^*(\boldsymbol{r})\}.\end{aligned} \tag{A.5}$$

On the other hand, the following calculation can be given starting from Eq. (A.3)

$$\begin{aligned}[\Psi_0^*\nabla^2\Psi_0 - \Psi_0\nabla^2\Psi_0^*] &= -\frac{2m_0}{\hbar^2}[\Psi_n^*H_{n0}\Psi_0 - \Psi_nH_{n0}^*\Psi_0^*]\\ &= -e^2\frac{2m_0}{\hbar^2}\left[\int \mathrm{d}\boldsymbol{r}_1\, G(\boldsymbol{r},\boldsymbol{r}_1)s(\boldsymbol{r},\boldsymbol{r}_1)\Psi_0^*(\boldsymbol{r})\Psi_0(\boldsymbol{r}_1)\right.\\ &\quad\left.-\int \mathrm{d}\boldsymbol{r}_1\, G^*(\boldsymbol{r},\boldsymbol{r}_1)s^*(\boldsymbol{r},\boldsymbol{r}_1)\Psi_0(\boldsymbol{r}_1)\Psi_0^*(\boldsymbol{r}_1)\right]\\ &= -e\frac{2m_0}{\hbar^2}\{[V'\Psi_0(\boldsymbol{r})]\psi_0(\boldsymbol{r}) - [V'\Psi_0(\boldsymbol{r})]^*\Psi_0(\boldsymbol{r})\}.\end{aligned} \tag{A.6}$$

A sum of Eqs. (A.5) and (A.6) gives

$$\int_{\Sigma} \mathrm{d}\boldsymbol{S}\cdot\boldsymbol{j} = 0,$$

which means the incoming intensity is equal to the out going intensity, the intensity is conserved.

Appendix B

Using the completeness relation of the crystal states,

$$\sum_{n} |a_n(\boldsymbol{R}_2)\rangle\langle a_n(\boldsymbol{R}_1)| = \delta(\boldsymbol{R}_2 - \boldsymbol{R}_1), \tag{B.1}$$

one has

$$\begin{aligned}
\sum_{n=1} [H_{n0}(\boldsymbol{r}_1)H^*_{n0}(\boldsymbol{r}_2)] &= \sum_{n=1} \langle a_0(\boldsymbol{R}_2)|H(\boldsymbol{r}_2,\boldsymbol{R}_2)|a_n(\boldsymbol{R}_2)\rangle\langle a_n(\boldsymbol{R}_1)|H(\boldsymbol{r}_1,\boldsymbol{R}_1)|a_0(\boldsymbol{R}_1)\rangle \\
&= \langle a_0(\boldsymbol{R}_2)|H(\boldsymbol{r}_2,\boldsymbol{R}_2)\left[\sum_{n=0} |a_n(\boldsymbol{R}_2)\rangle\langle a_n(\boldsymbol{R}_1)| - |a_0(\boldsymbol{R}_2)\rangle\langle a_0(\boldsymbol{R}_1)|\right]H(\boldsymbol{r}_1,\boldsymbol{R}_1)|a_0(\boldsymbol{R}_1)\rangle \\
&= \langle a_0(\boldsymbol{R}_2)|H(\boldsymbol{r}_2,\boldsymbol{R}_2)[\delta(\boldsymbol{R}_2 - \boldsymbol{R}_1) - |a_0(\boldsymbol{R}_2)\rangle\langle a_0(\boldsymbol{R}_1)|]H(\boldsymbol{r}_1,\boldsymbol{R}_1)|a_0(\boldsymbol{R}_1)\rangle \\
&= \langle a_0(\boldsymbol{R}_1)|H(\boldsymbol{r}_2,\boldsymbol{R}_1)H(\boldsymbol{r}_1,\boldsymbol{R}_1)|a_0(\boldsymbol{R}_1)\rangle \\
&\quad - \langle a_0(\boldsymbol{R}_2)|H(\boldsymbol{r}_2,\boldsymbol{R}_2)|a_0(\boldsymbol{R}_2)\rangle\langle a_0(\boldsymbol{R}_1)|H(\boldsymbol{r}_1,\boldsymbol{R}_1)|a_0(\boldsymbol{R}_1)\rangle
\end{aligned} \tag{B.2}$$

Using the Fourier transform of $H = -eV$, Eq. (B.2) is transformed into

$$\sum_{n\neq 0} [H_{n0}(\boldsymbol{r}_1)H^*_{n0}(\boldsymbol{r}_2)] = e^2\int \mathrm{d}\boldsymbol{Q}\int \mathrm{d}\boldsymbol{Q}'\,\exp[2\pi\mathrm{i}(\boldsymbol{r}_1\cdot\boldsymbol{Q} - \boldsymbol{r}_2\cdot\boldsymbol{Q}')]S'(\boldsymbol{Q},\boldsymbol{Q}'), \tag{B.3}$$

where the mixed dynamic form factor is given by (see Chapter 6 in Ref. [2])

$$\begin{aligned}
S'(\boldsymbol{Q},\boldsymbol{Q}') &= \sum_{\kappa}\sum_{\kappa'} \exp[2\pi\mathrm{i}(\boldsymbol{r}_{\kappa'}\cdot\boldsymbol{Q}' - \boldsymbol{r}_{\kappa}\cdot\boldsymbol{Q})] f^e_{\kappa}(\boldsymbol{Q}) f^e_{\kappa'}(\boldsymbol{Q}')\{\langle a_0|\exp[2\pi\mathrm{i}\boldsymbol{Q}\cdot(\boldsymbol{u}_{\kappa'} - \boldsymbol{u}_{\kappa})]|a_0\rangle \\
&\quad - \langle a_0|\exp(2\pi\mathrm{i}\boldsymbol{Q}\cdot\boldsymbol{u}_{\kappa'})|a_0\rangle\langle a_0|\exp(-2\pi\mathrm{i}\boldsymbol{Q}\cdot\boldsymbol{u}_{\kappa})|a_0\rangle\} \\
&= \sum_{\kappa}\sum_{\kappa'} \exp[2\pi\mathrm{i}(\boldsymbol{r}_{\kappa'}\cdot\boldsymbol{Q}' - \boldsymbol{r}_{\kappa}\cdot\boldsymbol{Q})] f^e_{\kappa}(\boldsymbol{Q}) f^e_{\kappa'}(\boldsymbol{Q}')\exp[-W_{\kappa}(\boldsymbol{Q}) - W_{\kappa'}(\boldsymbol{Q}')] \\
&\quad \times \{\exp[2F_{\kappa\kappa'}(\boldsymbol{Q},\boldsymbol{Q}')] - 1\}.
\end{aligned} \tag{B.4}$$

where

$$W_{\kappa}(\boldsymbol{Q}) = 2\pi^2\langle a_0|(\boldsymbol{u}_{\kappa}\cdot\boldsymbol{Q})^2|a_0\rangle, \tag{B.5}$$

and

$$F_{\kappa\kappa'}(\boldsymbol{Q},\boldsymbol{Q}') = 2\pi^2\langle a_0|(\boldsymbol{u}_{\kappa}\cdot\boldsymbol{Q})(\boldsymbol{u}_{\kappa'}\cdot\boldsymbol{Q}')|a_0\rangle. \tag{B.6}$$

$F_{\kappa\kappa'}$ is defined as a correlation function that is determined by the coupling between vibrations of the κ and κ' atoms.

In practice, the ground state $|a_0\rangle$ of the crystal is the phonon state at thermal equilibrium. To incorporate the statistical distribution of phonons in the ground state at a finite temperature, the calculations of Eq. (B.5) and (B.6) need to be modified to represent the expectation values. If the phonon state for a system containing a total of n_s phonons is denoted by $|n_s\rangle$, a weight factor $p(n_s)$ is added in Eqs. (B.5) and (B.6), resulting in

$$W_{\kappa}(\boldsymbol{Q}) = 2\pi^2\langle a_0|(\boldsymbol{Q}\cdot\boldsymbol{u}_{\kappa})^2|a_0\rangle = \sum_{n_s}\langle n_s|(\boldsymbol{Q}\cdot\boldsymbol{u}_{\kappa})^2|n_s\rangle p(n_s), \tag{B.7}$$

and

$$F_{\kappa\kappa'}(\boldsymbol{Q},\boldsymbol{Q}') = 2\pi^2\langle n_s|(\boldsymbol{u}_\kappa\cdot\boldsymbol{Q})(\boldsymbol{u}_{\kappa'}\cdot\boldsymbol{Q}')|n_s\rangle p(n_s), \tag{B.8}$$

where

$$p(n_s) = \frac{\exp[-(n_s+1/2)\hbar\omega_j/k_BT]}{\sum_{n_s=0}^{\infty}\exp[-(n_s+1/2)\hbar\omega_j/k_BT]} = [1-\exp(-\hbar\omega_j/k_BT)]\exp(-n_s\hbar\omega_j/k_BT). \tag{B.9}$$

A detailed calculation of W_κ and $F_{\kappa\kappa'}$ has been given in Refs. [2,14] using the harmonic oscillators model. Finally, comparing Eq. (B.4) with that obtained from the "frozen" lattice model reported elsewhere [14], yields

$$\sum_{n\neq 0}[H_{n0}(\boldsymbol{r}_1)H_{n0}^*(\boldsymbol{r}_2)] = e^2\langle\Delta V(\boldsymbol{r}_1)\Delta V(\boldsymbol{r}_2)\rangle. \tag{B.10}$$

Appendix C

From Eq. (14), one can perform the following calculation:

$$\begin{aligned}\Psi_0(\boldsymbol{r})\Psi_0^*(\boldsymbol{r}') = {}& \Psi_0^{(0)}(\boldsymbol{r})\Psi_0^{(0)*}(\boldsymbol{r}') + e^2\Psi_0^{(0)*}(\boldsymbol{r}')\int d\boldsymbol{r}_1\int d\boldsymbol{r}_2\; G(\boldsymbol{r},\boldsymbol{r}_1)G(\boldsymbol{r}_1,\boldsymbol{r}_2)s(\boldsymbol{r}_1,\boldsymbol{r}_2)\Psi_0^{(0)}(\boldsymbol{r}_2)\\ &+ e^2\Psi_0^{(0)}(\boldsymbol{r})\int d\boldsymbol{r}_1\int d\boldsymbol{r}_2\; G^*(\boldsymbol{r}',\boldsymbol{r}_1)G^*(\boldsymbol{r}_1,\boldsymbol{r}_2)s^*(\boldsymbol{r}_1,\boldsymbol{r}_2)\Psi_0^{(0)*}(\boldsymbol{r}_2)\\ &+ e^4\Psi_0^{(0)*}(\boldsymbol{r}')\int d\boldsymbol{r}_1\int d\boldsymbol{r}_2\int d\boldsymbol{r}_3\int d\boldsymbol{r}_4\; G(\boldsymbol{r},\boldsymbol{r}_1)G(\boldsymbol{r}_1,\boldsymbol{r}_2)G(\boldsymbol{r}_2,\boldsymbol{r}_3)G(\boldsymbol{r}_3,\boldsymbol{r}_4)s(\boldsymbol{r}_1,\boldsymbol{r}_2)s(\boldsymbol{r}_3,\boldsymbol{r}_4)\Psi_0^{(0)}(\boldsymbol{r}_4)\\ &+ e^4\Psi_0^{(0)}(\boldsymbol{r})\int d\boldsymbol{r}_1\int d\boldsymbol{r}_2\int d\boldsymbol{r}_3\int d\boldsymbol{r}_4\; G^*(\boldsymbol{r}',\boldsymbol{r}_1)G^*(\boldsymbol{r}_1,\boldsymbol{r}_2)G^*(\boldsymbol{r}_2,\boldsymbol{r}_3)G^*(\boldsymbol{r}_3,\boldsymbol{r}_4)s^*(\boldsymbol{r}_1,\boldsymbol{r}_2)\\ &\times s^*(\boldsymbol{r}_3,\boldsymbol{r}_4)\Psi_0^{(0)*}(\boldsymbol{r}_4) + \ldots\end{aligned} \tag{C.1}$$

In Eq. (15), the first term represents the elastically scattered wave and the second term is the diffuse scattering term(s). We preserve the form of the Bragg reflections that is given in Eq. (C.1) and substitute Eq. (C.1) into the second term of Eq. (15), which gives

$$\begin{aligned}\rho(\boldsymbol{r},\boldsymbol{r}) = {}& \Psi_0(\boldsymbol{r})\Psi_0^*(\boldsymbol{r}') + e^2\int d\boldsymbol{r}_1\int d\boldsymbol{r}_2\; G(\boldsymbol{r},\boldsymbol{r}_1)G^*(\boldsymbol{r}',\boldsymbol{r}_2)s(\boldsymbol{r}_1,\boldsymbol{r}_2)\Psi_0^{(0)*}(\boldsymbol{r}_2)\Psi_0^{(0)}(\boldsymbol{r}_1)\\ &+ e^4\int d\boldsymbol{r}_1\int d\boldsymbol{r}_2\int d\boldsymbol{r}_3\int d\boldsymbol{r}_4\; G(\boldsymbol{r},\boldsymbol{r}_1)G^*(\boldsymbol{r}',\boldsymbol{r}_2)G(\boldsymbol{r}_1,\boldsymbol{r}_3)G(\boldsymbol{r}_3,\boldsymbol{r}_4)s(\boldsymbol{r}_1,\boldsymbol{r}_2)s(\boldsymbol{r}_3,\boldsymbol{r}_4)\Psi_0^{(0)*}(\boldsymbol{r}_2)\Psi_0^{(0)}(\boldsymbol{r}_4)\\ &+ e^4\int d\boldsymbol{r}_1\int d\boldsymbol{r}_2\int d\boldsymbol{r}_3\int d\boldsymbol{r}_4\; G(\boldsymbol{r},\boldsymbol{r}_1)G^*(\boldsymbol{r}',\boldsymbol{r}_2)G^*(\boldsymbol{r}_2,\boldsymbol{r}_3)G^*(\boldsymbol{r}_3,\boldsymbol{r}_4)s(\boldsymbol{r}_1,\boldsymbol{r}_2)s^*(\boldsymbol{r}_3,\boldsymbol{r}_4)\Psi_0^{(0)}(\boldsymbol{r}_1)\Psi_0^{(0)*}(\boldsymbol{r}_4)\\ &+ e^6\int d\boldsymbol{r}_1\int d\boldsymbol{r}_2\int d\boldsymbol{r}_3\int d\boldsymbol{r}_4\int d\boldsymbol{r}_5\int d\boldsymbol{r}_6\; G(\boldsymbol{r},\boldsymbol{r}_1)G^*(\boldsymbol{r}',\boldsymbol{r}_2)G(\boldsymbol{r}_2,\boldsymbol{r}_3)G(\boldsymbol{r}_3,\boldsymbol{r}_4)G(\boldsymbol{r}_4,\boldsymbol{r}_5)G(\boldsymbol{r}_5,\boldsymbol{r}_6)\\ &\times s(\boldsymbol{r}_1,\boldsymbol{r}_2)s(\boldsymbol{r}_3,\boldsymbol{r}_4)s(\boldsymbol{r}_5,\boldsymbol{r}_6)\Psi_0^{(0)*}(\boldsymbol{r}_2)\Psi_0^{(0)}(\boldsymbol{r}_6)\\ &+ e^6\int d\boldsymbol{r}_1\int d\boldsymbol{r}_2\int d\boldsymbol{r}_3\int d\boldsymbol{r}_4\int d\boldsymbol{r}_5\int d\boldsymbol{r}_6\; G(\boldsymbol{r},\boldsymbol{r}_1)G^*(\boldsymbol{r}',\boldsymbol{r}_2)G^*(\boldsymbol{r}_2,\boldsymbol{r}_3)G^*(\boldsymbol{r}_3,\boldsymbol{r}_4)G^*(\boldsymbol{r}_4,\boldsymbol{r}_5)G^*(\boldsymbol{r}_5,\boldsymbol{r}_6)\\ &\times s(\boldsymbol{r}_1,\boldsymbol{r}_2)s^*(\boldsymbol{r}_3,\boldsymbol{r}_4)s^*(\boldsymbol{r}_5,\boldsymbol{r}_6)\Psi_0^{(0)}(\boldsymbol{r}_1)\Psi_0^{(0)*}(\boldsymbol{r}_6) + \ldots\end{aligned} \tag{C.2}$$

where the first term is the result of Bragg scattering, the second term is the first-order diffuse scattering, the third and the fourth terms are the second-order diffuse scattering, and the fourth and the sixth terms are the third-order diffuse scattering, etc. The split of the third and the fourth (or the fifth and the sixth) terms is due to the different variables $\boldsymbol{r}$ and $\boldsymbol{r}'$ introduced in the density matrix. All of the higher-order terms are included if one continues the iterative calculation.

Appendix D

For the convenience of the proof, the plane wave component is separated by defining $\bar{g}(\boldsymbol{r}, \boldsymbol{r}_1)$ as

$$G(\boldsymbol{r}, \boldsymbol{r}_1) \approx \exp[2\pi \mathrm{i} \boldsymbol{K}_0 \cdot (\boldsymbol{r} - \boldsymbol{r}_1)] \bar{g}(\boldsymbol{r}, \boldsymbol{r}_1), \tag{D.1}$$

thus for $z > z_1$ in the forward scattering

$$\bar{g}(\boldsymbol{r}, \boldsymbol{r}_1) = -\xi O_p(\boldsymbol{b}, z - z_1)\{\delta(\boldsymbol{b} - \boldsymbol{b}_1)\} = -\xi \int_0^z \mathrm{d}z' \, O_p(\boldsymbol{b}, z - z')\{\delta(\boldsymbol{b} - \boldsymbol{b}_1)\delta(z' - z_1)\}. \tag{D.2}$$

A direct differentiation of $\bar{g}(\boldsymbol{r}, \boldsymbol{r}_1)$ yields

$$\begin{aligned} \frac{\partial \bar{g}(\boldsymbol{r}, \boldsymbol{r}_1)}{\partial z} &= -\varsigma \left[\Xi + \frac{2m_0}{\hbar^2} eV_0 \right] \xi \int_0^z \mathrm{d}z' \, O_p(\boldsymbol{b}, z - z')\{\delta(\boldsymbol{b} - \boldsymbol{b}_1)\delta(z' - z_1)\} - \xi\{\delta(\boldsymbol{b} - \boldsymbol{b}_1)\delta(z - z_1)\} \\ &= \varsigma \left[\Xi + \frac{2m_0}{\hbar^2} eV_0 \right] \bar{g}(\boldsymbol{r}, \boldsymbol{r}_1) - \xi \delta(\boldsymbol{r} - \boldsymbol{r}_1). \end{aligned} \tag{D.3}$$

This is just the equation satisfied by $\bar{g}(\boldsymbol{r}, \boldsymbol{r}_1)$ under the small angle forward scattering approximation.

References

[1] J.C.H. Spence, J.M. Zuo, Electron Microdiffraction, Plenum Press, New York, 1992.
[2] Z.L. Wang, Elastic and Inelastic Scattering in Electron Diffraction and Imaging, Plenum Press, New York, 1995.
[3] H. Yoshioka, J. Phys. Soc. Japan 12 (1957) 618.
[4] P.H. Dederichs, Solid State Phys. 27 (1972) 135.
[5] A. Howie, R.M. Stern, Z. Naturforsch. 27 (1972) 382.
[6] C.J. Humphreys, P.B. Hirsch, Phil. Mag. 18 (1968) 115.
[7] G. Radi, Acta Cryst. A 26 (1970) 41.
[8] M.J. Whelan, J. Appl. Phys. 36 (1965) 2099.
[9] M.J. Whelan, J. Appl. Phys. 36 (1965) 2103.
[10] D. Van Dyck (1998), in preparation.
[11] Z.L. Wang, Phys. Rev. B 41 (1991) 12818.
[12] R.F. Loane, P. Xu, J. Silcox, Acta Cryst. A 47 (1991) 267.
[13] C. Dinges, A. Berger, H. Rose, Ultramicroscopy 60 (1995) 49.
[14] Z.L. Wang, Acta Cryst. A 51 (1995) 569.
[15] Z.L. Wang, Acta Cryst. A (1998), in press.
[16] Z.L. Wang, Acta Cryst. A 45 (1989) 636.
[17] D. Van Dyck, J. Danckaert, W. Coene, E. Selderslaghs, D. Broddin, J. Van Landuyt, S. Amelinckx, in: W. Krakow, M. O'Keefe (Eds.), Computer Simulation of Electron Microscope Diffraction and Images, The Minerals, Metals and Materials Soc., 1989, p. 107.
[18] Z.L. Wang, Acta Cryst. A 52 (1996) 717.
[19] H. Kohl, H. Rose, Adv. Electronics and Electron Phys. 65 (1985) 173.
[20] Z.L. Wang, Surf. Sci. 366 (1996) 377.
[21] Z.L. Wang, Phil. Mag. B 74 (1996) 733.
[22] S.L. Dudarev, D.D. Vvedensky, M.J. Whelan, Phys. Rev. B 50 (1994) 14525.
[23] Z.L. Wang, Phil. Mag. B 77 (1997) 787.

[24] D. Van Dyck, Adv. Electron. and Electron. Phys. (1985) 295.
[25] J.H. Chen, M. Op de Beeck, D. Van Dyck, Microsc. Microanal. Microstruct. 7 (1996) 27.
[26] J.H. Chen, D. Van Dyck, M. Op de Beeck, J. Van Landuyt, Ultramicroscopy 69 (1997) 219.
[27] J.H. Chen, Ph.D thesis, University of Anterwerpen, 1997.
[28] K. Kambe, C. Stampfl, Ultramicroscopy 55 (1994) 221.
[29] C.J. Humphreys, Rep. Prog. Phys. 42 (1979) 1825.
[30] K. Ishizuka, Acta Cryst. A 38 (1982) 773.
[31] J.H. Chen, D. Van Dyck, Acta Cryst. A (1997), in press.
[32] Z.L. Wang, Acta Cryst. A 46 (1990) 366.
[33] P. Rez, Acta Cryst. A 34 (1978) 48.
[34] D.M. Bird, Q.A. King, Acta Cryst. A 46 (1990) 202.
[35] G.R. Anstis, Acta Cryst. A 52 (1996) 450.
[36] L.M. Peng, G. Ren, S.L. Dudarev, M.J. Whelan, Acta Cryst. A 52 (1996) 456.
[37] L.M. Peng, G. Ren, S.L. Dudarev, M.J. Whelan, Acta Cryst. A 52 (1996) 257.
[38] A. Weickenmeier, H. Kohl, Acta Cryst. A 47 (1991) 590.